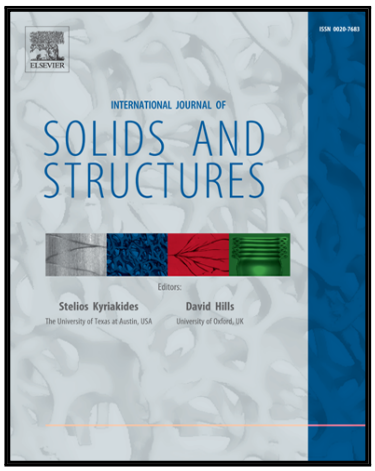

Computational Modeling of Interfacial Behaviors in Nanocomposite Materials

Liqiang Lin , Xiaodu Wang , Xiaowei Zeng

PII: S0020-7683(17)30072-0
DOI: 10.1016/j.ijsolstr.2017.02.029
Reference: SAS 9498

To appear in: *International Journal of Solids and Structures*

Received date: 19 June 2016
Revised date: 18 January 2017
Accepted date: 15 February 2017

Please cite this article as: Liqiang Lin , Xiaodu Wang , Xiaowei Zeng , Computational Modeling of Interfacial Behaviors in Nanocomposite Materials, *International Journal of Solids and Structures* (2017), doi: 10.1016/j.ijsolstr.2017.02.029

Computational Modeling of Interfacial Behaviors in Nanocomposite Materials

Liqiang Lin, Xiaodu Wang, Xiaowei Zeng*

Department of Mechanical Engineering, University of Texas at San Antonio, TX 78249

Abstract: Towards understanding the bulk material response in nanocomposites, an interfacial zone model was proposed to define a variety of material interface behaviors (e.g. brittle, ductile, rubber-like, elastic-perfectly plastic behavior etc.). It also has the capability to predict bulk material response though independently control of the interface properties (e.g. stiffness, strength, toughness). The mechanical response of granular nanocomposite (i.e. nacre) was investigated through modeling the "relatively soft" organic interface as an interfacial zone among "hard" mineral tablets and simulation results were compared with experimental measurements of stress-strain curves in tension and compression tests. Through modeling varies material interfaces, we found out that the bulk material response of granular nanocomposite was regulated by the interfacial behaviors. This interfacial zone model provides a possible numerical tool for qualitatively understanding of structure-property relationships through material interface design.

Keywords: Material interface modeling; organic interface; nacre; biological nanocomposite; polycrystalline structure

1. Introduction

Biological nanocomposites such as fish scale, bone and nacre are increasingly attracting attention from engineers and researchers due to their remarkable mechanical performances (Vernerey et al., 2014). In this kind of mineralized nanocomposites, the volume fraction of mineral generally is over 85vol% (Dastjerdi et al., 2013; Ritchie, 2011; Wang and Gupta, 2011). In some extreme cases, such as tooth enamel or shell of Strombus gigas, the volume fraction of mineral is up to 99vol% (Kamat et al., 2000; Yahyazadehfar and Arola, 2015). However, these biological nanocomposites exhibit outstanding strength and toughness with high contents of brittle minerals due to their ingenious design of microstructures. The universal microstructural feature of these

* Corresponding author.
E-mail address: xiaowei.zeng@utsa.edu (X. Zeng)

biological nanocomposites is that the brittle mineral tablets are bonded by "relatively soft" interfaces (Barthelat and Rabiei, 2011; Fratzl and Weinkamer, 2007; Gao, 2006; Ni et al., 2015; Vernerey et al., 2014). Thus, although the minerals are brittle, the "soft" interfaces could deflect the crack propagation and provide addition energy dissipation paths along the interfacial surfaces. Through the inspiration of wisdom and ingenious design in the biological nanocomposites, a number of artificial super materials have been fabricated (Bonderer et al., 2008; Deville et al., 2006; Finnemore et al., 2012; Munch et al., 2008).

To investigate how the interfacial behaviors and properties will determine the mechanical performance of nanocomposite materials, various experimental tests were conducted, it was found out that the toughness and strength of bulk materials can be improved through different mechanisms, e.g. the interface shear deformation (Barthelat and Espinosa, 2007; Gupta et al., 2006; Mercer et al., 2006), interlocking of nano-asperities and micro-scale waviness (Espinosa et al., 2011; Wang et al., 2001), mineral bridging (Smith et al., 1999; Song et al., 2003). In the meanwhile, different theoretical models have been proposed to study contributions of interfacial interaction on the mechanical response of bulk materials (Okumura, 2015). The shear lag model was borrowed to study the transfer of stress through tablets and interfaces under the tensile loading (Gao et al., 2003; Jackson et al., 1988; Kotha et al., 2001). The elastic energy model was applied to study the effects of interface stiffness and volume fraction on the stiffness and toughness of bulk materials (Okumura and De Gennes, 2001). In addition, various numerical models were applied to study the role of interfaces in determining the mechanical properties of bulk materials. The bilinear cohesive zone model (Geubelle and Baylor, 1998) was used to investigate the effects of mineral-collagen interface behavior on microdamage accumulation in lamellar bone tissues(Luo et al., 2011). The exponential cohesive zone model (Van den Bosch et al., 2006; Xu and Needleman, 1994) was employed to determine the independent roles of enzymatic and non-enzymatic cross-linking on the mechanical behavior of a mineralized collagen fibril (Siegmund et al., 2008). Despite broad studies have been conducted to scrutinize the interface contributions on the high mechanical performance of nanocomposites, it still has not been fully elucidated how the interfacial behaviors and properties determine the mechanical response of bulk materials. From experimental perspective, it is difficult to directly observe the contributions of interfacial properties on the mechanical response of bulk material because the deformation process involves multiscale underlying mechanisms in strengthening toughness and

strength (Barthelat and Rabiei, 2011; Peterlik et al., 2006). On the other hand, there are currently no comprehensive interfacial zone models to capture the different interfacial behaviors in determination of the bulk material response.

The aim of current work is to develop an interfacial zone model to describe difference material interface behaviors to predict the bulk material response through material interface design. In this work, the characteristics and features of the proposed interfacial zone model are discussed firstly. Then, the mechanical behavior of granular nanocomposite (i.e. nacre) was studied using the proposed interfacial zone model to model the interfacial behaviors of nanocomposite. The simulation results provide insights on how the interfacial behaviors and interfacial damage pattern control the bulk material response.

2. Development of the interfacial zone model

The granular biological nanocomposites (e.g. nacre) have the universal structure in which the hard aragonite crystals are bonded by "relatively soft" interfaces (Fig. 1). Although the interface is relatively weak and its volume fraction is very low, it has high impact on the mechanical performance of bulk material. During the interface debonding process, the interface could undergo normal or shear deformation. To describe the interface deformation behaviors, an interfacial zone model was proposed to mimic various interfacial behaviors. The traction-separation relations in normal and shear directions were used to govern the interfacial behaviors as shown in Fig. 2, which include four deformation stages in normal traction-separation law: compressive contact stage $(0{\sim}\delta_0)$, elastic stage $(\delta_0{\sim}\delta_{dn})$, damage stage $(\delta_{dn}{\sim}\delta_{fn})$ and complete failure stage $(\delta_{fn}{\sim}+\infty)$. In the shear traction-separation law, it has the similar deformation stages (elastic stage $(0{\sim}\delta_{dt})$, damage stage $(\delta_{dt}{\sim}\delta_{ft})$ and complete failure stage $(\delta_{ft}{\sim}\infty)$) with symmetry in both positive and negative directions. The interface toughness is the area under the traction-separation curve and the normal and shear interface toughness are respectively defined as:

$$\emptyset_n = \int_{\delta_0}^{\delta_{\mathrm{fn}}} \mathbf{T}\,\mathrm{d}\boldsymbol{\delta} \tag{1}$$

$$\emptyset_t = \int_{0}^{\delta_{\mathrm{ft}}} \mathbf{T}\,\mathrm{d}\boldsymbol{\delta} \tag{2}$$

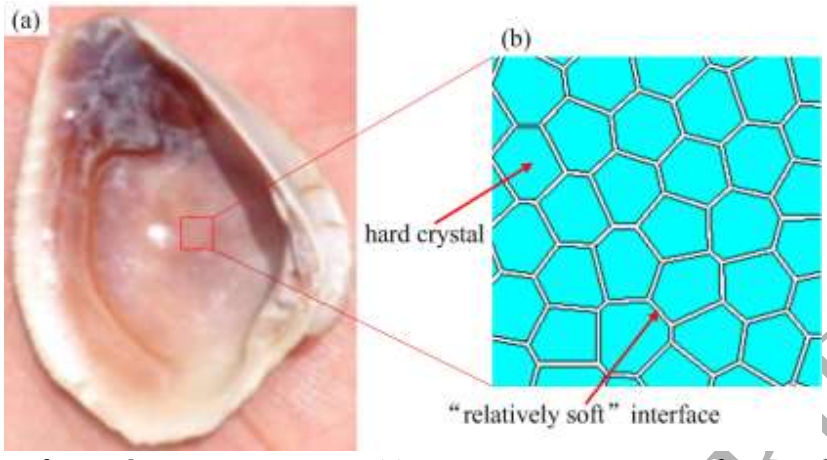

Fig. 1 Schematic of granular nanocomposite: (a) macroscopic structure of nacre, (b) microscopic structure of nacre

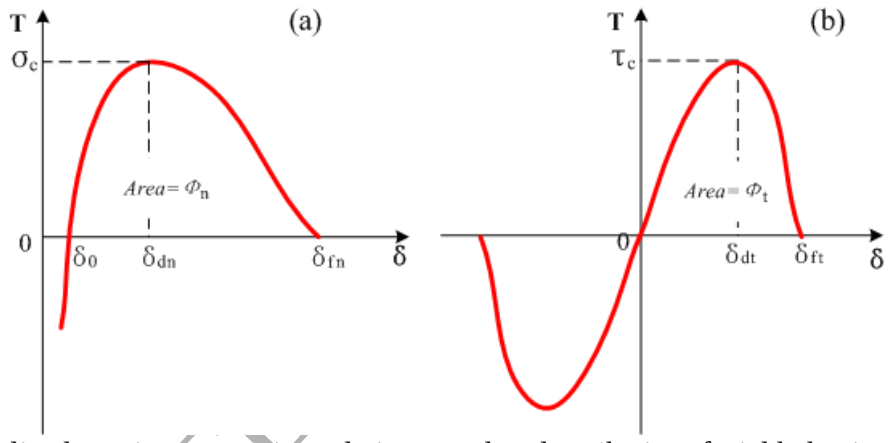

Fig. 2 Generalized traction-separation relations used to describe interfacial behaviors: (a) normal direction, (b) tangential direction

In the interfacial interaction, it is not necessary for normal and shear interaction always to have mutual effects on each other. For instance, the uncramping and unfolding of molecule in collagen fibrils due to stretching might not involve shear interaction (Meyers et al., 2013). For this reason, we presented an uncoupled interfacial zone model in this study for interfacial modeling. Based on Xu and Needleman's exponential cohesive traction-separation law (Xu and Needleman, 1994), an interfacial zone model was proposed to model different interfacial behaviors. The proposed interfacial traction-separation laws take the following form:

$$T_n = \begin{cases} \sigma_c \left(\frac{\Delta_n - \delta_0}{\delta_{dn} - \delta_0}\right) \exp(1) exp\left(-\frac{\Delta_n - \delta_0}{\delta_{dn} - \delta_0}\right) & \Delta_n \leq \delta_{dn} \\ \sigma_c \left(\frac{\delta_{fn} - \Delta_n}{\delta_{fn} - \delta_n}\right)^{p_n} & \delta_{dn} < \Delta_n < \delta_{fn} \\ 0 & \Delta_n \geq \delta_{fn} \end{cases} \quad (3)$$

$$T_t = \begin{cases} \tau_c \sqrt{\exp(1)} \left(\frac{\Delta_t}{\delta_{dt}}\right) exp\left(-\frac{\Delta_t^2}{2\delta_{dt}^2}\right) & 0 \leq |\Delta_t| \leq \delta_{dt} \\ \tau_c \frac{\Delta_t}{|\Delta_t|} \left(\frac{\delta_{ft} - |\Delta_t|}{\delta_{ft} - \delta_{dt}}\right)^{p_t} & \delta_{dt} < |\Delta_t| < \delta_{ft} \\ 0 & \Delta_n \geq \delta_{ft} \end{cases} \quad (4)$$

where σ_c and τ_c are cohesive strength in normal and tangential direction, respectively; and δ_{dn} and δ_{dt} are critical separation. The δ_{fn} and δ_{ft} are normal and tangential failure separation, respectively. The δ_0 is the equilibrium position and $\exp(1) = 2.71828$. The shape parameters (p_n, p_t) are introduced to describe different interfacial behaviors (or different traction-separation curve shapes), e.g. brittle, ductile, rubber-like behavior etc. In the model, the variables Δ_n and Δ_t represent normal and tangential separation, respectively.

The interfacial traction-separation laws for different positive and negative value of shape parameters (p_n, p_t) are plotted in Fig. 3 and Fig. 4. It can be seen from Fig. 3 that the proposed interfacial zone model has the exponential properties before damage initiation position(δ_{dn} *or* δ_{dt}). In the damage stage ($\delta_{dn} \sim \delta_{fn}$ *or* $\delta_{dt} \sim \delta_{ft}$), the model shows different shapes with different shape parameters (p_n, p_t). When the shape parameter is between zero to one, the current model demonstrates a convex softening shape. When the shape parameters are equal to one, the damage behavior of current model represents a linear relation. When the shape parameters are greater than one, the damage behavior has a concave shape. As a special case, when $p_n = 0$ or $p_t = 0$, it represents elastic-perfectly plastic behavior in normal or in shear direction (Fig. 3). In addition, when shape parameters (p_n, p_t) are taking as negative values, it can be seen from Fig. 4 that the interface shows a rubber-like behavior.

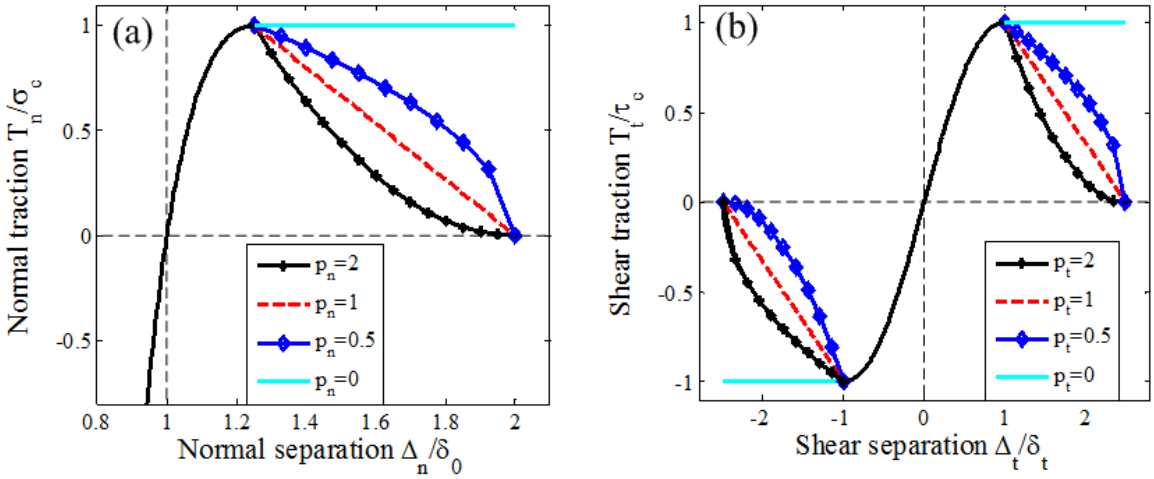

Fig. 3 Different interfacial behaviors with positive shape parameters (p_n, p_t)

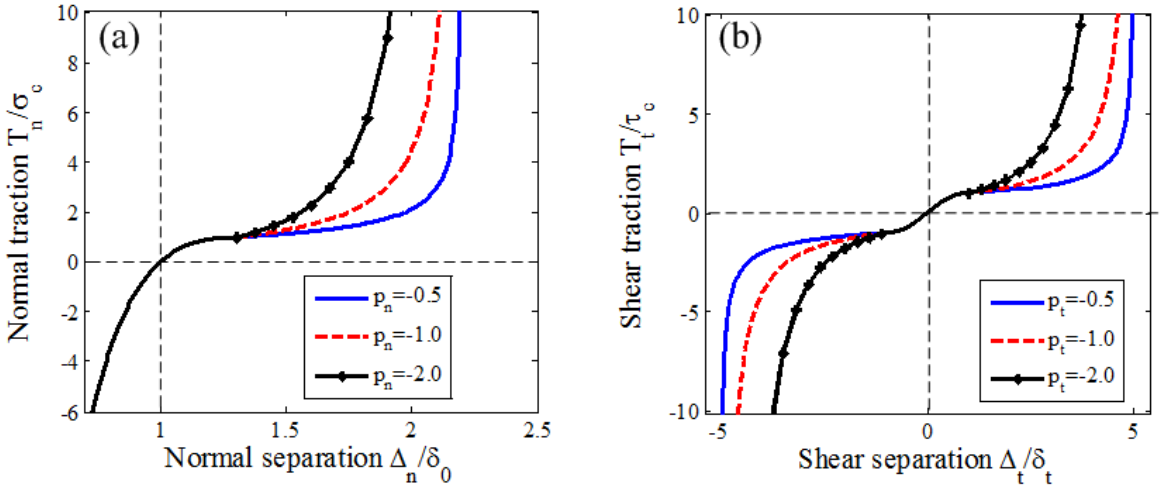

Fig. 4 Different interfacial behaviors with negative shape parameters (p_n, p_t)

In addition, the stiffness of the interface at the equilibrium position is defined as:

$$K_n = \frac{dT_n}{d\Delta_n} = \sigma_c \exp(1)\left[\left(\frac{1}{\delta_{dn}-\delta_0}\right) exp\left(-\frac{\Delta_n-\delta_0}{\delta_{dn}-\delta_0}\right) - \left(\frac{\Delta_n-\delta_0}{(\delta_{dn}-\delta_0)^2}\right) exp\left(-\frac{\Delta_n-\delta_0}{\delta_{dn}-\delta_0}\right)\right]\Big|_{\Delta_n=\delta_0} = \frac{\sigma_c \exp(1)}{\delta_{dn}-\delta_0} \quad (5)$$

$$K_t = \frac{dT_t}{d\Delta_t} = \tau_c\sqrt{\exp(1)}\left[\frac{1}{\delta_{dt}} exp\left(-\frac{\Delta_t^2}{2\delta_{dt}^2}\right) - \frac{\Delta_t^2}{\delta_{dt}^3} exp\left(-\frac{\Delta_t^2}{2\delta_{dt}^2}\right)\right]\Big|_{\Delta_t=0} = \frac{\tau_c\sqrt{\exp(1)}}{\delta_{dt}} \quad (6)$$

Eqs. (5) and (6) suggest that a smaller value of $(\delta_{dn} - \delta_0)$ or δ_{dt} would result in a higher interface stiffness in normal or tangential direction. Thus, $(\delta_{dn} - \delta_0)$ and δ_{dt} can be used to tune the interface stiffness in the normal and tangential directions.

In the proposed interfacial zone model, there are five independent parameters (σ_c, δ_{dn}, δ_0, δ_{fn} and p_n) in normal direction and four independent parameters (τ_c, δ_{dt}, δ_{ft} and p_t) in tangential direction to manipulate different interfacial properties and behaviors. The interface toughness ($\emptyset_n, \emptyset_t$) can be readily determined from the traction-separation curves.

To test the proposed interfacial zone model, a two-dimensional geometry of granular nanocomposite was generated in which the mineral crystals are bounded by an interfacial zone. The proposed traction-separation laws were employed to mimic different interfacial behaviors in the granular nanocomposite. The proposed interfacial model was verified through a comparing study with experimental measurements (*i.e.* stress-strain relation). On the other hand, by using this model, the bulk mechanical behavior of granular nanocomposite can be predicted through material interface design.

3. Geometry model and materials

3.1 Geometry model of granular nanocomposite

A well-known example of granular nanocomposites is nacre. The nacre is composed of aragonite ($CaCO_3$) crystals, which are organized in polygonal tablet, arranged in a thin layer of interfaces (Fig. 5). For simplicity while ensuring reasonable accuracy, a two-dimensional (2D) model of $CaCO_3$ crystals bounded through a thin interface (Fig. 5) was generated in this study to represent the microstructure of nacre. Briefly, polygonal shaped $CaCO_3$ crystals were first generated using the Centroidal Voronoi tessellation method in a 2D geometric model (Lin et al., 2014b). Then, an interfacial zone was created to represent the organic interface between the $CaCO_3$ crystals by recessing the edges of each grain cell in parallel towards the centroid of the grains with a designated distance (Fig. 5). Based on the previous study regarding the minimum representative elementary volume (Evesque and Adjémian, 2002), 100 grains were required for the proposed 2D model to ensure consistent outcomes. In this study, roughly one hundred and forty four (144) $CaCO_3$ grains were generated in each representative model. Based on the existing information on the thickness (20nm~35nm) (Barthelat and Espinosa, 2007; Barthelat et al., 2006; Dastjerdi et al., 2013; Lopez et al., 2014) and volume fraction (~5% vol) (Barthelat et al., 2007; Song et al., 2003) of the organic interface in nacre, the interfacial zone thickness in the model was set to be 20nm and the specimen size was set to be $L_x \times L_y = 8400nm \times 8400nm$.

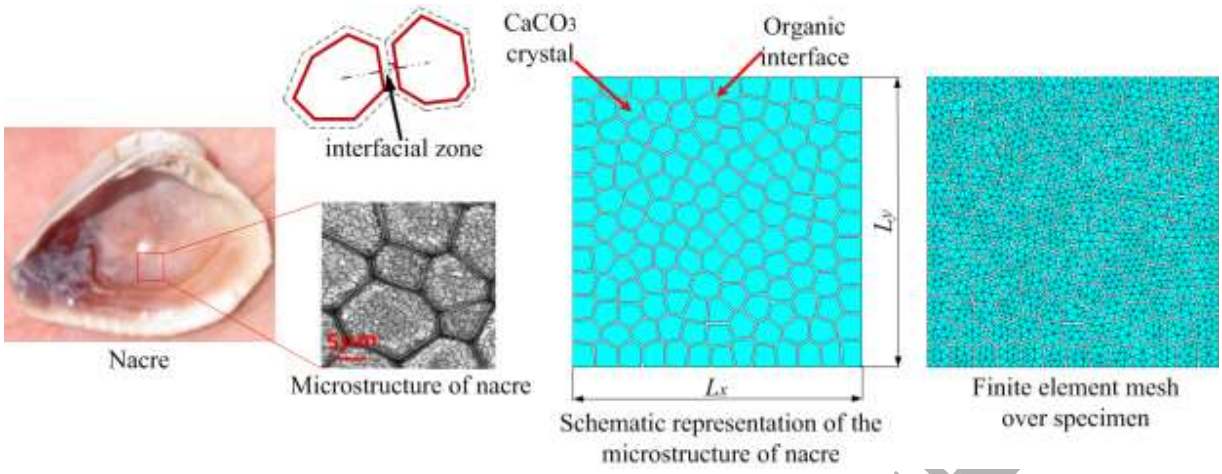

Fig. 5 2D geometry model of a granular nanocomposite. The interfacial zone was generated by recessing the outline of the original Voronoi cells (dash line) to form the new outline of the mineral grain (solid line). The grains in specimen were meshed by triangular element.

3.2 Material properties

According to the material properties of aragonite crystal reported in the literatures (Askarinejad and Rahbar, 2015; Barthelat et al., 2006; Hrabánková et al., 2013; Zhang and Chen, 2013)，the material properties of $CaCO_3$ were set to be: Young's modulus $E = 100\text{GPa}$, Poisson's ratio $v = 0.28$, mineral density $\rho = 3{,}190 kg/m^3$. The soft interface in nacre contains different molecules and a direct experimental measurement of interface properties and behaviors at nanoscale is very challenging. In this study, the mechanical behaviors of the interface were simplified and governed by the traction-separation laws, which can be defined through those independent parameters described earlier. Those independent interfacial parameters will be estimated based on the experimental data and numerical simulation results reported in the literatures for different interfacial properties of nacre (Barthelat et al., 2007; Espinosa et al., 2009; Evans et al., 2001; Lin and Meyers, 2009; Meyers et al., 2013; Smith et al., 1999; Wang et al., 2001).

4 Numerical simulations

4.1 FEM implementations

Following standard procedures and neglecting the body force, the principle of virtual work of finite element formulation is written as:

$$\int_{\Omega} \mathbf{P}: \delta\mathbf{F} d\Omega - \int_{\Gamma_{inter}} \mathbf{T}^{inter} \cdot \delta\Delta dS = \int_{\Gamma_{ext}} \overline{\mathbf{T}} \cdot \delta\mathbf{u} dS - \int_{\Omega} \rho\ddot{\mathbf{u}} \cdot \delta\mathbf{u} d\Omega \quad (7)$$

where Ω, Γ_{inter}, Γ_{ext} are the volume, interface boundary and external traction boundary of element in the reference configuration, respectively; **P** is the first Piola-Kirchhoff stress tensor; **F** is the deformation gradient; Δ denotes the interfacial displacement jump across the interfaces; $\overline{\mathbf{T}}$ denotes the external traction vector and $\mathbf{T}^{inter}$ is the interfacial bonding traction vector; ρ represents the material density in the reference configuration. The Newmark β method was applied for the explicit time integration with $\beta = 0$ and $\gamma = 0.5$ (Hughes et al., 1979).

In this study, the organic interface behaviors were governed by the traction-separation laws described earlier. The $CaCO_3$ grains were meshed using triangular elements. All simulations were implemented using a custom-made finite element package, which had been developed by Zeng and his co-workers (Li et al., 2012; Lin et al., 2014a; Lin et al., 2015; Lin and Zeng, 2015; Zeng and Li, 2010, 2012). Uniaxial load (tensile or compressive loading) was applied to the finite element model by assigning a uniform displacement on the top and bottom edges of the model (Lin et al., 2014a), with the right and left side of the specimen being set free.

4.2 Comparison study of the interfacial zone model via an elastic-perfectly plastic behavior

The organic interface in the nacre is a thin layer of biopolymer, which has the capability of very large extension through sequential uncramping and unfolding of modules (Mohanty et al., 2008; Smith et al., 1999). It was noted that experimental data did not show a significant hardening over the large stretching test. In addition, the interface provided the slipping possibility between minerals (Wang et al., 2001). Some researchers described the interface to have a long plateau after yield point (Barthelat et al., 2007; Evans et al., 2001). Hence, we assumed that the interface has an elastic-perfectly plastic behavior. Specifically, the normal critical displacement ($\delta_{dn} - \delta_0$) at the interface was set to be 0.6nm. This value was estimated by assuming that the tensile yield stain of the interface was 3.0% based on the information reported in literatures (Barthelat et al., 2007; Dastjerdi et al., 2013). The data reported by (Smith et al., 1999) illustrated that some molecules with large stretching capability is present in the interface. According to the study of (Mohanty et al., 2008; Smith et al., 1999), the effective displacement of plateau region is from 30nm to 100nm. Through parametric study and sensitivity test, it was found that the simulation

results matched with experimental data when we set normal failure separation $(\delta_{fn} - \delta_0) = 30\text{nm}$. Hence, the normal failure separation $(\delta_{fn} - \delta_0)$ at the interface was estimated to be 30nm in this study by assuming that the tensile failure strain of the interface was approximately 150%. In the absence of experimental data on the interfacial shear behavior, we assumed the traction-separation relation in tangential direction is similar to the one in normal direction. The critical shear separation δ_{dt} was set to be 0.6nm and the failure shear separation δ_{ft} was set to be 30nm. The strength in normal direction was set to be $\sigma_c = 110\text{MPa}$ and the shear interface strength was set to be $\tau_c = 40\text{MPa}$ based on the experimental data reported in literatures(Barthelat and Espinosa, 2007; Espinosa et al., 2009; Evans et al., 2001; Lin and Meyers, 2009). The details of the interface parameters were listed in Table 1 and the curves of the traction-separation laws were plotted in Fig. 6.

Table 1 Parameters of interface property with elastic-perfectly plastic behavior

$\sigma_n(\text{MPa})$	110
$(\delta_{dn} - \delta_0)(nm)$	0.6
$(\delta_{fn} - \delta_0)(nm)$	30
p_n	0.0
$\tau_t(\text{MPa})$	40
$\delta_{dt}(nm)$	0.6
$\delta_{ft}(nm)$	30
p_t	0.0

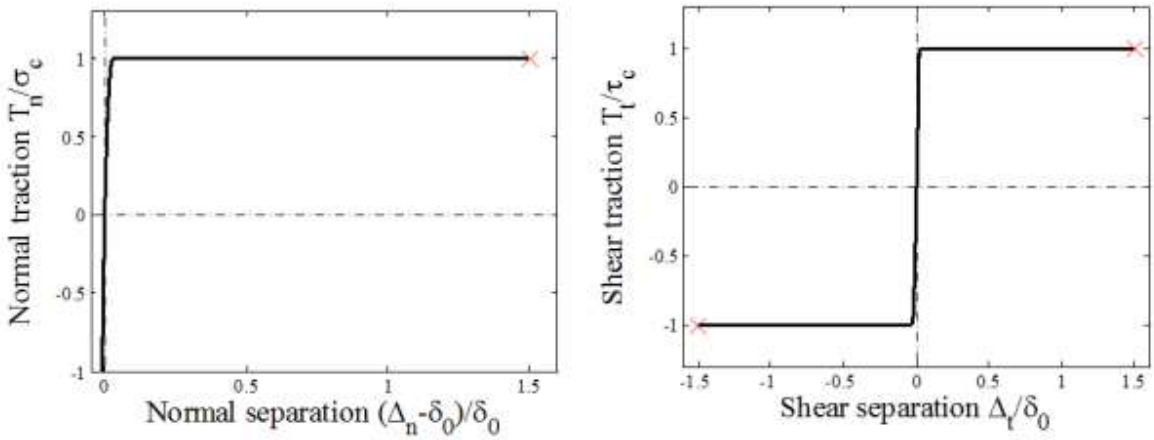

Fig. 6 The traction-separation relations with respect to elastic-perfectly plastic interfacial behavior: (a) normal direction, and (b) shear direction

In current study, grains in the specimen were meshed by triangular element (Fig. 5). Based on the previous convergence test of similar models (Lin et al., 2017; Lin et al., 2016), the mesh size in current work is around 150nm and the time step is $\Delta t = 1 \times 10^{-10} s$. We have plotted the stress-strain curves after calculations, the stress-strain curves in the early post yield state agreed well with experimental measurements as shown in Fig. 7. The average stress was compiled as mean ± standard deviation in which 6 samples with random polycrystalline grain distribution are considered in the calculation. The bulk stress showed an initial strain hardening after yield point in tension (Fig. 7). However, in compression, the stress-strain curve showed a relatively linear pattern until failure. The average yield stress of approximately 100MPa in tension is very close to the experimental yield stress of 105MPa. The ultimate stress was approximately 452±93MPa in compression, and the experimental value of 370MPa when testing was discontinued lies in the range. In addition, the stiffness obtained from the simulation matched with the experimental measurement value at approximately 70GPa. The agreement between the simulation results and experimental data suggested that the proposed interfacial zone model has the capability to capture the characteristics and features of the interfacial behaviors.

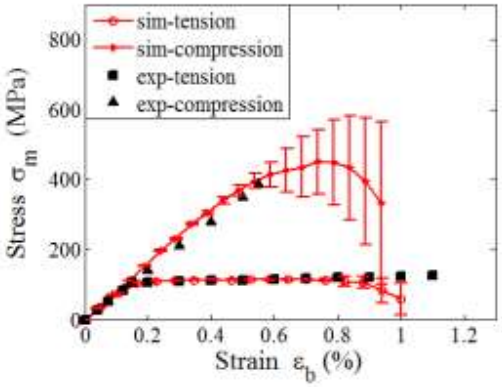

Fig. 7 The stress-strain relations in tension and compression tests: the sim-tension represented simulation result in tension; the sim-compression represented simulation result in compression; the exp-tension denoted experimental result in tension; the exp-compression denoted experimental result in compression. The experimental results in abalone nacre were reported in Wang et al. (Wang et al., 2001).

4.3 Prediction of bulk material response via a rubber-like interfacial behavior model

As we know, different biopolymer may show different material behaviors. For instance, the spider silk shows a rubber-like behavior(Meyers et al., 2013). This kind of biopolymer also showed high plastic deformation. To understand the effects of interface behavior on the

mechanical response of biological nanocomposites, we designed a case by assuming that the interface possessed rubber-like behavior in a biological nanocomposite. The interface parameters were estimated based on the information reported in literatures (Lin and Meyers, 2009; Meyers et al., 2013). The designed interface properties were set to be: $\sigma_c = 130\text{MPa}, \tau_c = 40\text{MPa}$, $(\delta_{dn} - \delta_0) = 3nm$, $\delta_{dt} = 3nm$ at 15% yield point and $(\delta_{fn} - \delta_0) = 15nm$, $\delta_{ft} = 15nm$ at 75% failure position, $p_n = p_t = -1.5$ based on the properties reported in the literatures (Lin and Meyers, 2009; Meyers et al., 2013). The details of the interface parameters were listed in Table 2 and the curves of the traction-separation laws were plotted in Fig. 8. According to the data reported by (Meyers et al., 2013), the failure strain of interface with rubber-like behavior in this case was set as 0.63. From the traction-separation curve, we can readily determine the ultimate stress of interface with rubber-like behavior to be 1.4GPa.

Table 2 Parameters of interface property with rubber-like behavior

σ_n(MPa)	130
$(\delta_{dn} - \delta_0)(nm)$	3
$(\delta_{fn} - \delta_0)(nm)$	15
p_n	-1.5
τ_t(MPa)	40
$\delta_{dt}(nm)$	3
$\delta_{ft}(nm)$	15
p_t	-1.5

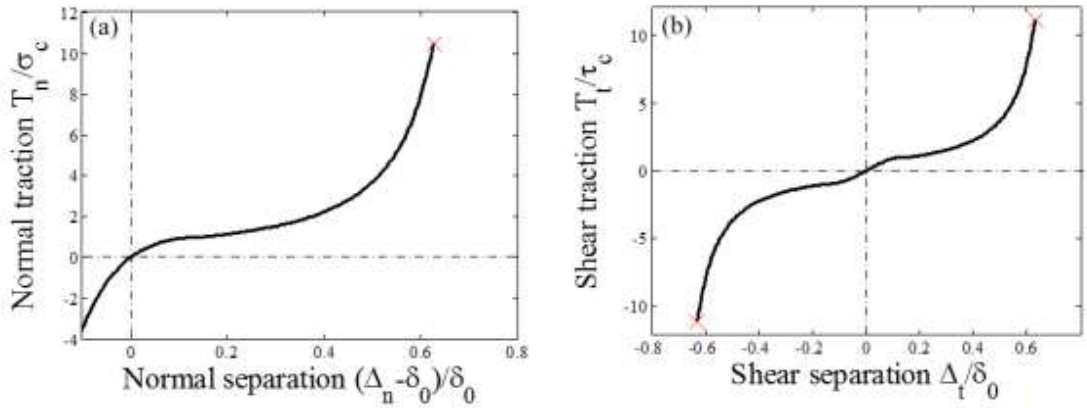

Fig. 8 The traction-separation relations with respect to rubber-like interface behavior: (a) normal direction, and (b) shear direction

In observation of the stress-strain curves for tension and compression tests, it was found that the bulk stress with rubber-like interface also showed a rubber-like behavior in stress-strain relation under tensile loading (Fig. 9(a)). This result may explain that the stress-strain relation of whelk eggs always presents a trend of rubber-like behavior under tension test in different temperature condition (Meyers et al., 2013) possibly because the organic interface between the minerals inside the whelk eggs has an overall rubber-like property. In compression test, however, the stress-strain curve showed a relatively linear response until failure (Fig. 9(b)).

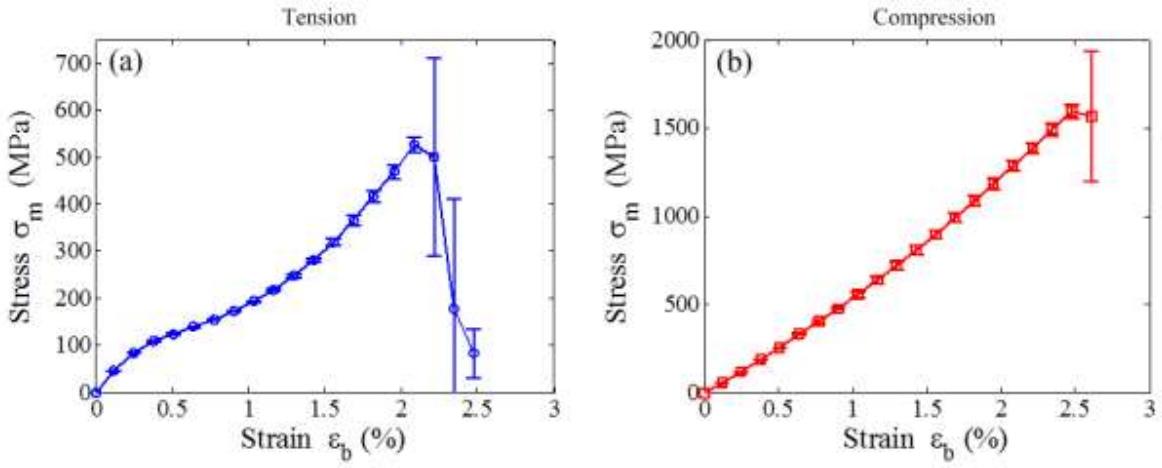

Fig. 9 The stress-strain relation in tension and compression for rubber-like interface: (a) tension; (b) compression.

4.4 Deformation & failure pattern from different loading conditions

It has been investigated that the loading mode dependence of nacre mechanical behavior is manifested (Evans et al., 2001; Wang and Gupta, 2011; Wang et al., 2001). The ultimate stress of nacre in tension is smaller than the one in compress (Jacobs, 1990). On the other hand, the stress-strain curve of nacre shows highly nonlinear behavior in tension(Barthelat and Espinosa, 2007; Evans et al., 2001; Wang et al., 2001), whereas it shows linear response in compression (Barthelat et al., 2006; Evans et al., 2001; Wang et al., 2001). Furthermore, the dilatation band was formed among intertablets when nacre is in tension(Wang et al., 2001). This is highly indicated that the fracture mechanism of nacre in tension vs. compression.

Through analysis of the fracture pattern in the specimen, we found that the cracks were initiated at the interface perpendicular to the loading direction when the model was loaded in tension (Fig. 10 and Fig. 11). When the damage at the interfaces started to initiate, the stress σ_{22} released

within the damage interface zone region. As the loading kept increasing, cracks nucleated and coalesced, and finally traveled transversely passing through the specimen (Fig. 10 and Fig. 11). It seems that there is a tendency for the crack initiation, nucleation and coalescence mainly in mode I. This phenomenon is analogous to the observation of "dilatation bands" in the nacre under tension test (Wang et al., 2001).

When the specimen loaded in compression, intergranular cracks propagated along an inclined angle *via* relative sliding between the mineral crystals (Fig. 12 and Fig. 13). This deformation/failure tendency of inclined crack propagation within interfaces allowed more energy dissipation during the damage process.

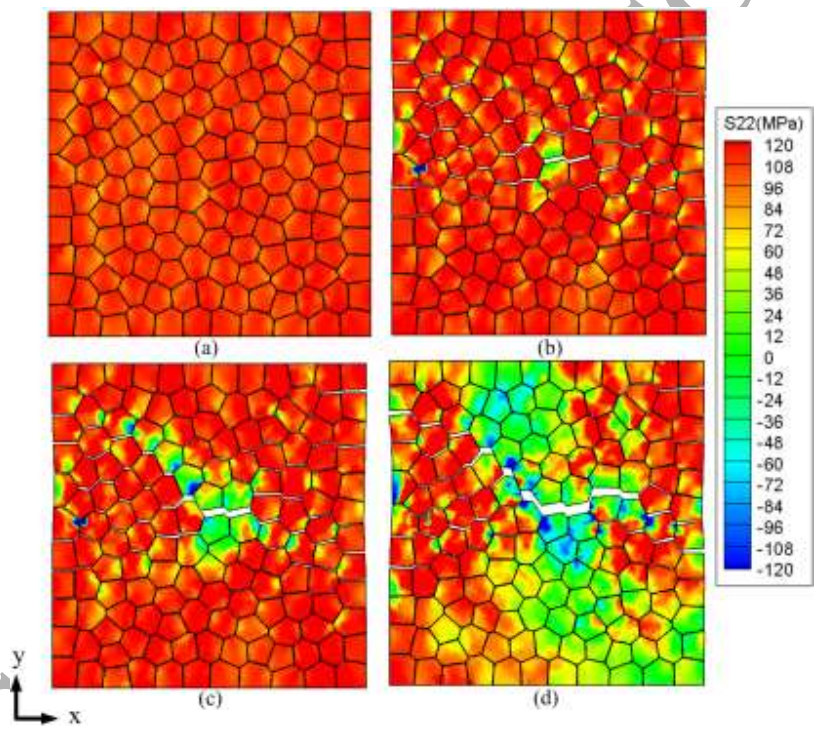

Fig. 10 Snapshots of stress distribution(σ_{22}) with elastic-perfectly plastic interface under tensile loading: (a) $\varepsilon_b = 0.19\%$, (b) $\varepsilon_b = 1.02\%$ (crack initiation), (c) $\varepsilon_b = 1.05\%$ (crack nucleation), (d) $\varepsilon_b = 1.1\%$ (crack coalescence)

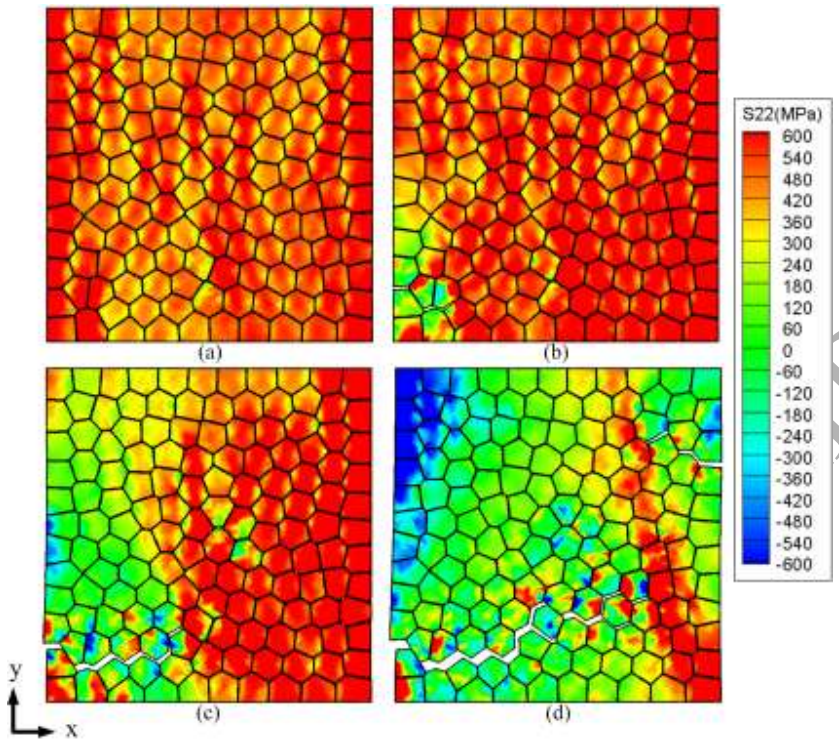

Fig. 11 Snapshots of stress distribution(σ_{22}) with rubber-like interface under tensile loading: (a) $\varepsilon_b = 2.07\%$, (b) $\varepsilon_b = 2.26\%$ (crack initiation), (c) $\varepsilon_b = 2.34\%$ (crack nucleation), (d) $\varepsilon_b = 2.38\%$ (crack coalescence)

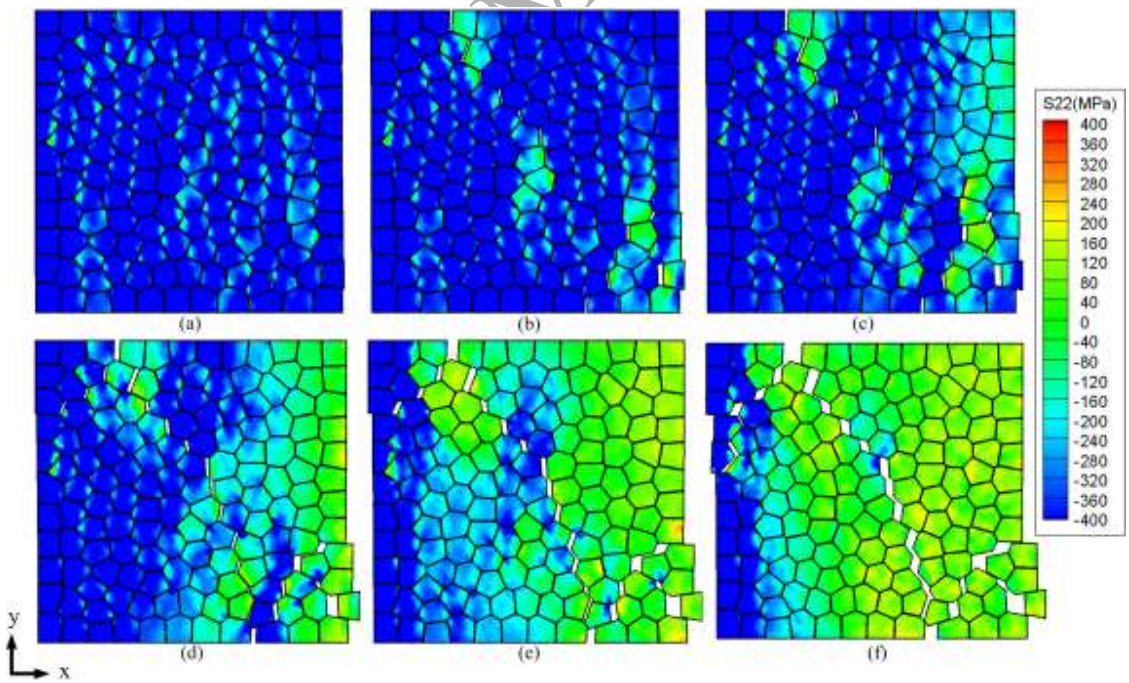

Fig. 12 Snapshots of stress distribution (σ_{22}) with elastic-perfectly plastic interface under compressive loading: (a) $\varepsilon_b = 0.78\%$, (b) $\varepsilon_b = 0.83\%$ (crack initiation), (c) $\varepsilon_b = 0.85\%$,

(d) $\varepsilon_b = 0.88\%$ (crack propagation along an incline angle within interface) (e) $\varepsilon_b = 0.92\%$, (f) $\varepsilon_b = 0.99\%$

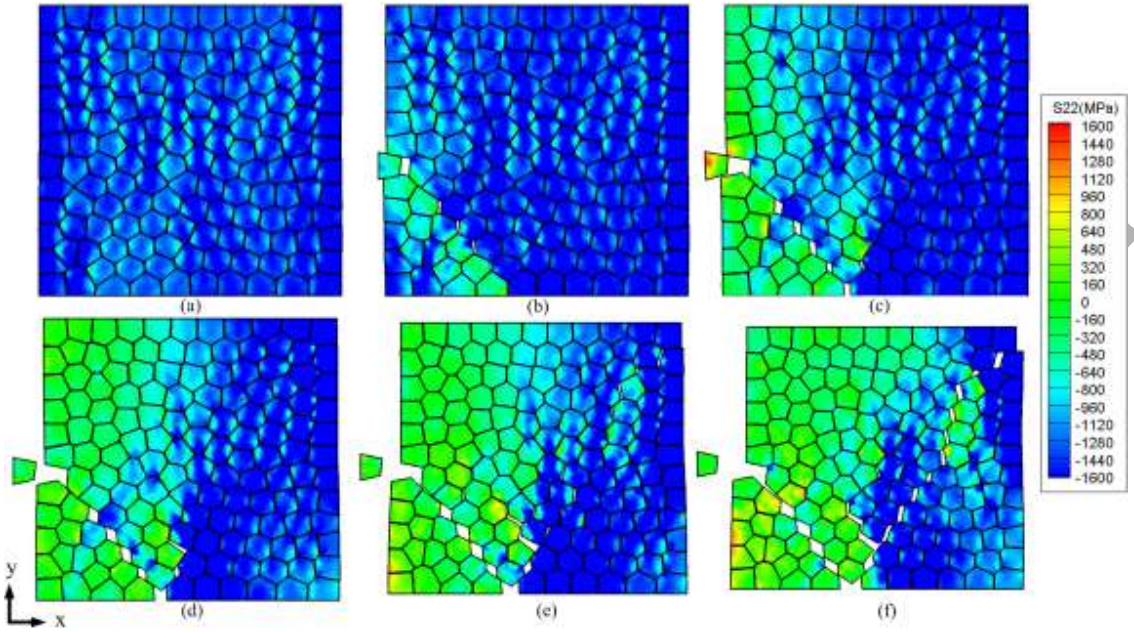

Fig. 13 Snapshots of stress distribution (σ_{22}) with rubber-like interface under compressive loading: (a) $\varepsilon_b = 2.34\%$, (b) $\varepsilon_b = 2.49\%$ (crack initiation), (c) $\varepsilon_b = 2.55\%$ (crack propagation along an incline angle within interface), (d) $\varepsilon_b = 2.57\%$, (e) $\varepsilon_b = 2.58\%$, (f) $\varepsilon_b = 2.61\%$

4.5 Bulk Material Response vs. Different Interfacial Behaviors

To further prove that interface behavior directly influences the bulk material response, we conducted three simulations by assuming that the interface possessed a brittle, elastic-perfectly plastic and rubber-like behavior in a biological nanocomposite, as shown in Fig. 14. The details of the interface parameters were listed in Table 3. Through these studies, we explored the contribution of interfacial properties on the bulk material response. It is found that the bulk stress-strain curves are very similar to the interfacial behaviors in tension(Fig. 15), suggesting that the interface behavior directly dictates the bulk material response.

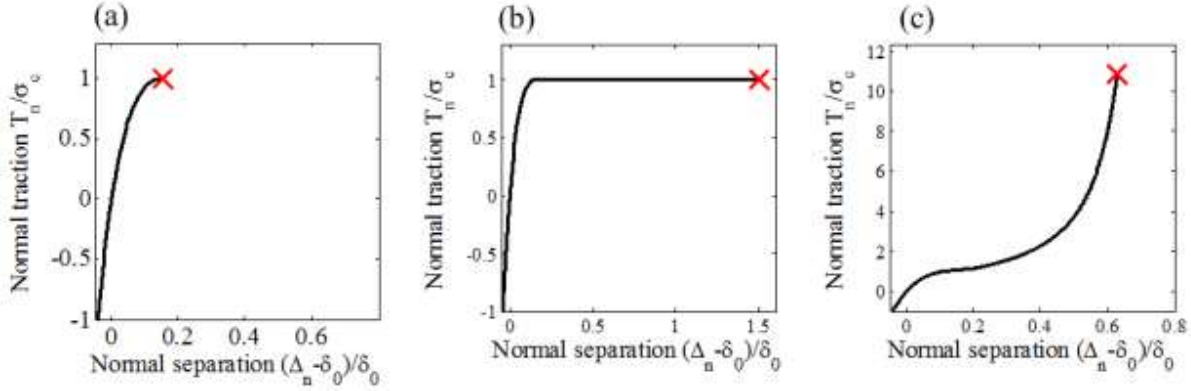

Fig. 14 The traction-separation relations with respect to different interfacial behaviors: (a) brittle, (b) elastic-perfectly plastic, (c) rubber-like.

Table 3 Parameters of interface property with different behaviors

	brittle	elastic perfectly plastic	rubber-like
σ_n(MPa)	130	130	130
$(\delta_{dn}-\delta_0)(nm)$	3	3	3
$(\delta_{fn}-\delta_0)(nm)$	3	30	15
p_n	-----	0	-1.5
τ_t(MPa)	40	40	40
$\delta_{dt}(nm)$	3	3	3
$\delta_{ft}(nm)$	3	30	15
p_t	--------	0	-1.5

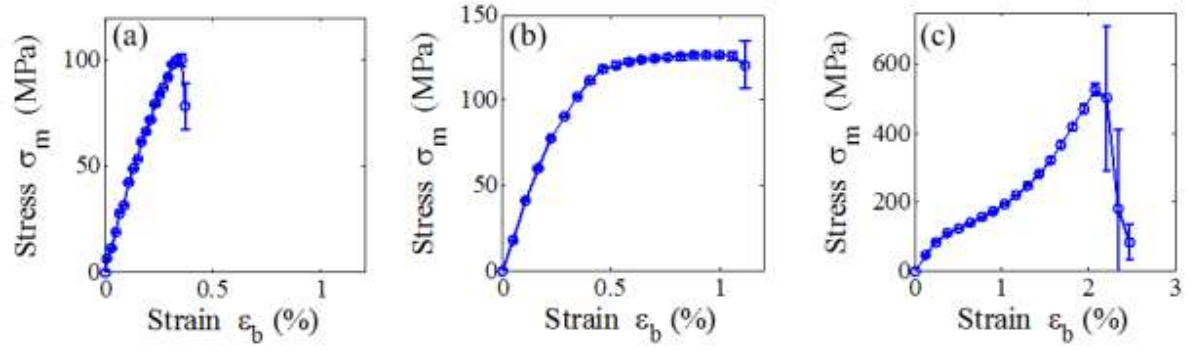

Fig. 15 The stress-strain relation of bulk material with different interfacial properties: (a) interface with brittle behavior; (b) interface with elastic perfectly plastic behavior; (c) interface with rubber-like behavior.

5. Discussion and Conclusions

In this study, we have reported an interfacial zone model for interface modeling in granular nanocomposites to study the bulk material response. The proposed interfacial model has the capability to describe different interfacial material behaviors, e.g. brittle, ductile, elastic-perfectly plastic and rubber-like behaviors through adjusting the control parameters.

Via comparison with experimental data, the stress-strain curves of simulation in the early post yield state agreed well with experimental measurements (Fig. 7). From the simulation results, we observed that the bulk stress-strain relation represented a rubber-like response with rubber-like interface behavior in tension, but bulk stress-strain showed a linear behavior in compression (Fig. 9). The simulation results also captured the damage process in a 2D nacre specimen. The loading mode dependence of the mechanical behavior of granular nanocomposites is manifested in the distinct deformation mode of the organic interface; that is, intergranular opening mode in tension and intergranular sliding mode in compression (Fig. 10-Fig. 13).

From fracture pattern (Fig. 10-Fig. 13) and the stress-strain relation analysis (Fig. 7 and Fig. 9), we observed that the bulk material behavior was regulated by the interface properties. The possible reason is that the interface carried the most loads under tensile loading due to its weak strength, which is easier to transfer loads to adjacent interfaces after it damaged along the interface in normal direction. Thus the interface behavior dominated the bulk material response. However, in compression, the interface could provide facility for the $CaCO_3$ crystals to continually slide along the interface till shear damage. Under compressive loading, the interfaces are mainly in compression. Due to the relatively linear behavior of interfaces under compression in normal direction, it might be the reason that the stress-strain curves showed a linear relation until failure in compression. Also, $CaCO_3$ is a linear elastic material, which may have contributions on the linear material response.

There are several limitations associated with current work. Firstly, a 2D plane strain model is used in the study of nacre, which may not be fully representative of 3D cases. Although 3D models composed of multiple layers, the inner plane fracture between mineral tablets is still the dominant failure mode in the structure based on experimental observations (Evans et al., 2001; Wang et al., 2001). In the early post yield state, the sliding between inter-layers might have minor effects on the bulk mechanical response, thus the current 2D plane strain model is

presumably only sufficient in capturing the early stage of post yield behaviors. Secondly, the organic interface properties are simply estimated based on the experimental observations and related information reported in the literatures, which do not consider complex chemical bonding and environment of organic-inorganic interface and may be used only for qualitative analysis. Nonetheless, the results of this study indicate that the proposed interfacial zone model is still able to capture the major deformation behavior of nacre, which may give rise to the insights on the mechanisms of superior tough and strong mechanical properties of nacre.

The proposed interfacial zone model provides a numerical tool to study bulk material response through defining different material interface behaviors. In addition, by adjusting the controllable parameters in the current interfacial zone model, we could independently control the interface stiffness, toughness, and mechanical strength in normal and shear directions. Through different interfacial behavior modeling by the proposed model, it is indicated that the bulk material response is largely determined by interfacial behavior. Through the model and simulation study, we could predict the bulk material behavior by interfacial property. The main point of this paper is to demonstrate the capability of the interfacial zone model and we believe the model can be used to design artificial tunable nanocomposite materials through material interface design.

Acknowledgements

This work is partially supported by a grant from National Institutes of Health (Grant No. R21AR066925), a grant from National Science Foundation (Grant No. CMMI-1538448)**,** and a grant from the University of Texas at San Antonio, Office of the Vice President for Research.

References

Askarinejad, S., Rahbar, N., 2015. Toughening mechanisms in bioinspired multilayered materials. Journal of The Royal Society Interface 12, 20140855.

Barthelat, F., Espinosa, H., 2007. An experimental investigation of deformation and fracture of nacre–mother of pearl. Experimental mechanics 47, 311-324.

Barthelat, F., Li, C.-M., Comi, C., Espinosa, H.D., 2006. Mechanical properties of nacre constituents and their impact on mechanical performance. Journal of Materials Research 21, 1977-1986.

Barthelat, F., Rabiei, R., 2011. Toughness amplification in natural composites. Journal of the Mechanics and Physics of Solids 59, 829-840.

Barthelat, F., Tang, H., Zavattieri, P., Li, C.-M., Espinosa, H., 2007. On the mechanics of mother-of-pearl: a key feature in the material hierarchical structure. Journal of the Mechanics and Physics of Solids 55, 306-337.

Bonderer, L.J., Studart, A.R., Gauckler, L.J., 2008. Bioinspired design and assembly of platelet reinforced polymer films. Science 319, 1069-1073.

Dastjerdi, A.K., Rabiei, R., Barthelat, F., 2013. The weak interfaces within tough natural composites: experiments on three types of nacre. Journal of the mechanical behavior of biomedical materials 19, 50-60.

Deville, S., Saiz, E., Nalla, R.K., Tomsia, A.P., 2006. Freezing as a path to build complex composites. Science 311, 515-518.

Espinosa, H.D., Juster, A.L., Latourte, F.J., Loh, O.Y., Gregoire, D., Zavattieri, P.D., 2011. Tablet-level origin of toughening in abalone shells and translation to synthetic composite materials. Nature communications 2, 173.

Espinosa, H.D., Rim, J.E., Barthelat, F., Buehler, M.J., 2009. Merger of structure and material in nacre and bone–Perspectives on de novo biomimetic materials. Progress in Materials Science 54, 1059-1100.

Evans, A., Suo, Z., Wang, R., Aksay, I., He, M., Hutchinson, J., 2001. Model for the robust mechanical behavior of nacre. Journal of Materials Research 16, 2475-2484.

Evesque, P., Adjémian, F., 2002. Stress fluctuations and macroscopic stick-slip in granular materials. The European Physical Journal E 9, 253-259.

Finnemore, A., Cunha, P., Shean, T., Vignolini, S., Guldin, S., Oyen, M., Steiner, U., 2012. Biomimetic layer-by-layer assembly of artificial nacre. Nature communications 3, 966.

Fratzl, P., Weinkamer, R., 2007. Nature's hierarchical materials. Progress in Materials Science 52, 1263-1334.

Gao, H., 2006. Application of fracture mechanics concepts to hierarchical biomechanics of bone and bone-like materials. International Journal of Fracture 138, 101-137.

Gao, H., Ji, B., Jäger, I.L., Arzt, E., Fratzl, P., 2003. Materials become insensitive to flaws at nanoscale: lessons from nature. Proceedings of the national Academy of Sciences 100, 5597-5600.

Geubelle, P.H., Baylor, J.S., 1998. Impact-induced delamination of composites: a 2D simulation. Composites Part B: Engineering 29, 589-602.

Gupta, H.S., Seto, J., Wagermaier, W., Zaslansky, P., Boesecke, P., Fratzl, P., 2006. Cooperative deformation of mineral and collagen in bone at the nanoscale. Proceedings of the National Academy of Sciences 103, 17741-17746.

Hrabánková, I., Frýda, J., Šepitka, J., Sasaki, T., Frýdová, B., Lukeš, J., 2013. Mechanical properties of deep-sea molluscan shell. Computer methods in biomechanics and biomedical engineering 16, 287-289.

Hughes, T.J., Pister, K.S., Taylor, R.L., 1979. Implicit-explicit finite elements in nonlinear transient analysis. Computer Methods in Applied Mechanics and Engineering 17, 159-182.

Jackson, A., Vincent, J., Turner, R., 1988. The mechanical design of nacre. Proceedings of the Royal Society of London B: Biological Sciences 234, 415-440.

Jacobs, D.K., 1990. Sutural pattern and shell stress in Baculites with implications for other cephalopod shell morphologies. Paleobiology 16, 336-348.

Kamat, S., Su, X., Ballarini, R., Heuer, A., 2000. Structural basis for the fracture toughness of the shell of the conch Strombus gigas. Nature 405, 1036-1040.

Kotha, S., Li, Y., Guzelsu, N., 2001. Micromechanical model of nacre tested in tension. Journal of materials science 36.

Li, S., Zeng, X., Ren, B., Qian, J., Zhang, J., Jha, A.K., 2012. An atomistic-based interphase zone model for crystalline solids. Computer Methods in Applied Mechanics and Engineering 229, 87-109.

Lin, A.Y.-M., Meyers, M.A., 2009. Interfacial shear strength in abalone nacre. Journal of the mechanical behavior of biomedical materials 2, 607-612.

Lin, L., Dhanawade, R., Zeng, X., 2014a. Numerical simulations of dynamic fracture growth based on a cohesive zone model with microcracks. Journal of Nanomechanics and Micromechanics 4, B4014003.

Lin, L., Samuel, J., Zeng, X., Wang, X., 2017. Contribution of extrafibrillar matrix to the mechanical behavior of bone using a novel cohesive finite element model. Journal of the Mechanical Behavior of Biomedical Materials 65, 224-235.

Lin, L., Wang, X., Zeng, X., 2014b. Geometrical modeling of cell division and cell remodeling based on Voronoi tessellation method. CMES: Computer Modeling in Engineering & Sciences 98, 203-220.

Lin, L., Wang, X., Zeng, X., 2015. The role of cohesive zone properties on intergranular to transgranular fracture transition in polycrystalline solids. International Journal of Damage Mechanics, 1056789515618732.

Lin, L., Wang, X., Zeng, X., 2016. An improved interfacial bonding model for material interface modeling. Engineering Fracture Mechanics.

Lin, L., Zeng, X., 2015. Computational modeling and simulation of spall fracture in polycrystalline solids by an atomistic-based interfacial zone model. Engineering fracture mechanics 142, 50-63.

Lopez, M.I., Martinez, P.E.M., Meyers, M.A., 2014. Organic interlamellar layers, mesolayers and mineral nanobridges: Contribution to strength in abalone (Haliotis rufescence) nacre. Acta biomaterialia 10, 2056-2064.

Luo, Q., Nakade, R., Dong, X., Rong, Q., Wang, X., 2011. Effect of mineral–collagen interfacial behavior on the microdamage progression in bone using a probabilistic cohesive finite element model. Journal of the mechanical behavior of biomedical materials 4, 943-952.

Mercer, C., He, M., Wang, R., Evans, A., 2006. Mechanisms governing the inelastic deformation of cortical bone and application to trabecular bone. Acta Biomaterialia 2, 59-68.

Meyers, M.A., McKittrick, J., Chen, P.-Y., 2013. Structural biological materials: critical mechanics-materials connections. science 339, 773-779.

Mohanty, B., Katti, K.S., Katti, D.R., 2008. Experimental investigation of nanomechanics of the mineral-protein interface in nacre. Mechanics Research Communications 35, 17-23.

Munch, E., Launey, M.E., Alsem, D.H., Saiz, E., Tomsia, A.P., Ritchie, R.O., 2008. Tough, bio-inspired hybrid materials. Science 322, 1516-1520.

Ni, Y., Song, Z., Jiang, H., Yu, S.-H., He, L., 2015. Optimization design of strong and tough nacreous nanocomposites through tuning characteristic lengths. Journal of the Mechanics and Physics of Solids 81, 41-57.

Okumura, K., 2015. Strength and toughness of biocomposites consisting of soft and hard elements: A few fundamental models. MRS Bulletin 40, 333-339.

Okumura, K., De Gennes, P.-G., 2001. Why is nacre strong? Elastic theory and fracture mechanics for biocomposites with stratified structures. The European Physical Journal E 4, 121-127.

Peterlik, H., Roschger, P., Klaushofer, K., Fratzl, P., 2006. From brittle to ductile fracture of bone. Nature materials 5, 52-55.

Ritchie, R.O., 2011. The conflicts between strength and toughness. Nature materials 10, 817-822.

Siegmund, T., Allen, M.R., Burr, D.B., 2008. Failure of mineralized collagen fibrils: modeling the role of collagen cross-linking. Journal of biomechanics 41, 1427-1435.

Smith, B.L., Schäffer, T.E., Viani, M., Thompson, J.B., Frederick, N.A., Kindt, J., Belcher, A., Stucky, G.D., Morse, D.E., Hansma, P.K., 1999. Molecular mechanistic origin of the toughness of natural adhesives, fibres and composites. Nature 399, 761-763.

Song, F., Soh, A., Bai, Y., 2003. Structural and mechanical properties of the organic matrix layers of nacre. Biomaterials 24, 3623-3631.

Van den Bosch, M., Schreurs, P., Geers, M., 2006. An improved description of the exponential Xu and Needleman cohesive zone law for mixed-mode decohesion. Engineering Fracture Mechanics 73, 1220-1234.

Vernerey, F.J., Musiket, K., Barthelat, F., 2014. Mechanics of fish skin: A computational approach for bio-inspired flexible composites. International Journal of Solids and Structures 51, 274-283.

Wang, R., Gupta, H.S., 2011. Deformation and fracture mechanisms of bone and nacre. Annual Review of Materials Research 41, 41-73.

Wang, R., Suo, Z., Evans, A., Yao, N., Aksay, I., 2001. Deformation mechanisms in nacre. Journal of Materials Research 16, 2485-2493.

Xu, X.-P., Needleman, A., 1994. Numerical simulations of fast crack growth in brittle solids. Journal of the Mechanics and Physics of Solids 42, 1397-1434.

Yahyazadehfar, M., Arola, D., 2015. The role of organic proteins on the crack growth resistance of human enamel. Acta biomaterialia 19, 33-45.

Zeng, X., Li, S., 2010. A multiscale cohesive zone model and simulations of fractures. Computer Methods in Applied Mechanics and Engineering 199, 547-556.

Zeng, X., Li, S., 2012. Application of a multiscale cohesive zone method to model composite materials. International Journal of Multiscale Computational Engineering 10, 391-405.

Zhang, N., Chen, Y., 2013. Nanoscale plastic deformation mechanism in single crystal aragonite. Journal of Materials Science 48, 785-796.